Journal of Veterinary Internal Medicine, 2026, 40(3), aalag080
https://doi.org/10.1093/jvimsj/aalag080
Original Research | Equine Cardiology

Delta (Δ) 12-lead electrocardiography and vectorcardiography to identify the origin of focally induced atrial and ventricular premature depolarizations in horses

Ellen Paulussen[1,*], Gunther van Loon[1], Eva Buschmann[1], Ingrid Vernemmen[1], Tammo Delhaas[2], Annelies Decloedt[1], Glenn Van Steenkiste[1]

[1]Equine Cardioteam Ghent, Department of Internal Medicine, Reproduction and Population Medicine, Faculty of Veterinary Medicine, Ghent University, Merelbeke, Belgium
[2]Department of Biomedical Engineering, Cardiovascular Research Institute Maastricht (CARIM), Maastricht University, Maastricht, The Netherlands
*Corresponding author: Ellen Paulussen, Equine Cardioteam Ghent, Salisburylaan 133, Merelbeke 9820, Belgium (ellen.paulussen@ugent.be).

Abstract

Background: **Cardiac arrhythmias are common in horses, but their clinical and prognostic relevance remains poorly defined. Despite the importance of localization for diagnosis and treatment, noninvasive methods to identify arrhythmogenic foci are limited.**

Hypothesis/Objectives: **Evaluate the ability of delta (Δ) 3- and 12-lead ECGs and 2-dimensional (2D) and 3-dimensional (3D) vectorcardiography (VCG) to identify the site of origin of focally induced atrial and ventricular premature depolarizations in horses.**

Animals: **Eight healthy horses underwent 2 electrophysiological studies, 1 standing, and 1 under general anesthesia.**

Methods: **Premature atrial and ventricular complexes were induced by intracardiac pacing at 29 anatomical sites. Simultaneous Δ 12-lead ECG and VCG recordings were obtained. Mean vector directions were analyzed, and classification accuracy was assessed at the chamber, regional, and site-specific levels.**

Results: **Distinct pacing sites produced reproducible and location-specific activation patterns. For differentiating left- from right-sided origins, 3D-VCG had 99% and 82% accuracies for ventricular and atrial origins, respectively. The simplified Δ-based 2D-VCG also showed strong performance on the chamber level, with accuracies of 94% and 78%, respectively. Accuracy was lower for fine-grained intra-chamber localization, especially in the atria.**

Conclusions and clinical importance: **Although 3D-VCG offers superior spatial resolution, 2D-VCG provides a good balance between diagnostic accuracy and practical applicability, especially for left- vs right-sided localization. Combined Δ 12-lead ECG and VCG enables accurate, noninvasive chamber-level localization of arrhythmia origins in horses. Standardized application in larger cohorts with naturally occurring arrhythmias may support targeted ablation strategies and improve arrhythmia management and sudden cardiac death risk stratification.**

Keywords arrhythmias, equine, multiple-lead ECG, pacing

Abbreviations Δ, delta; APC, atrial premature complex; Bpm, beats per minute; EAM, electro-anatomical mapping; MEA, mean electrical axis; LA, left atrium; LV, left ventricle; RA, right atrium; RMS, root mean square; RV, right ventricle; SR, sinus rhythm; VCG, vectorcardiogram/-graphy; VPC, ventricular premature complex

Received: October 9, 2025. **Revised:** March 30, 2026. **Accepted:** April 3, 2026

Introduction

In human medicine, the 12-lead ECG is a cornerstone in the diagnostic evaluation of arrhythmias, because known changes in morphology help to localize the site of origin. This localization determines the therapeutic strategy and influences long-term prognosis.[1] For example, in human medicine, ventricular tachycardia originating from the outflow tracts in a structurally normal heart generally has a benign prognosis, whereas tachycardia arising from other areas with myocardial scar tissue is associated with a significantly higher risk of sudden cardiac death.[1]

Cardiac arrhythmias are common in horses, yet their clinical and prognostic relevance often remains unclear.[2,3] Accurate identification of the anatomical origin of arrhythmias would improve effective diagnosis and treatment.[4,5] Surface ECG remains the primary diagnostic tool. Although 12-lead ECG recordings offer enhanced insights into arrhythmia origins in human patients and small animals, their application in horses has been limited because of technical challenges and inconsistent results.[6] Historically, most 12-lead ECG configurations used in horses were derived from configurations used in humans, and did not align well with the unique anatomical structure and position of the equine heart, potentially contributing to unreliable outcomes.[6–11] Recent advancements have introduced improved 12-lead ECG configurations tailored to the equine heart's electrical axis, enhancing diagnostic reliability.[6,12] In addition, vectorcardiography (VCG) synthesizes cardiac electrical activity into a 3-dimensional (3D) representation, facilitating the interpretation of the 12-lead ECG.[7,12]

Our objective was to determine if 2-dimensional (2D) and 3D-VCG-derived P wave and QRS complex characteristics, obtained from a Δ 3-lead and 12-lead ECG, respectively, could be used to identify the anatomical origin of pacing-induced atrial and ventricular premature complexes (APCs and VPCs).

Materials and methods

Our study was part of a larger study, including the follow-up of transseptal puncture,[13] evaluating the feasibility of transthoracic ultrasound guidance of intracardiac catheters[4] and multiple catheter recordings to investigate atrial depolarization patterns during sinus rhythm (SR) and induced premature atrial complexes.[14]

Study sample and data acquisition

Eight horses participated in the study: 4 warmbloods, 2 warmblood crossbreeds, and 2 trotters, with a mean age of 16 $\pm$ 8 years and a mean body weight of 510 $\pm$ 40 kg. Echocardiography indicated only mild valvular regurgitation and cardiac measurements within normal limits.[15] A 24-h ECG showed normal SR in all horses. Each horse underwent 2 electrophysiological studies involving the placement of multiple decapolar catheters (Webster CS Catheter, Biosense Webster, Irvine, California) at predetermined locations. All pacing locations are shown in Figure 1. All catheters were positioned using transthoracic echocardiographic guidance with final locations confirmed by 3D electroanatomical mapping (EAM) using the EnSite Precision Cardiac Mapping system (Abbott, Zaventem, Belgium).[4] Detailed information on sedation protocols, medication, and general anesthesia is provided in Supplementary File S1.

Right heart

In the first procedure, catheter positioning in the right heart was performed on standing, sedated horses. A Δ 12-lead ECG (Labsystem Pro v2.6, Boston Scientific, Diegem, Belgium) was continuously recorded throughout the procedure. The Delta 12-lead configuration is illustrated in Figure 2.[12]

In the right jugular vein, a decapolar catheter (Webster CS Catheter, Biosense Webster, Diegem, Belgium) was advanced through a fixed-curve sheath (HeartSpan, Merit Medical, Etterbeek, Belgium) into the coronary sinus and further into the great cardiac vein for left atrial (LA) signal acquisition.[4,16] In the left jugular vein, an 8.5 Fr bidirectional deflectable guiding sheath (Senovo Bi-Flex, Biotronik, Vilvoorde, Belgium) was introduced, through which a 7 Fr loop electrophysiology catheter (Inquiry Optima, Abbott, Zaventem, Belgium) was inserted to map the right atrium (RA). Catheters were placed using transthoracic echocardiographic guidance as described previously,[4] and position was verified by 3D EAM. Once the 3D EAM had been created, the loop catheter was removed.

Additional sheaths were inserted into the left jugular vein for the placement of decapolar recording catheters. A fixed-curve sheath was used for catheter placement at the medially located myocardial sleeves of the caudal vena cava, caudal to the fossa ovalis, at the most caudally obtainable electrogram site.[17] Two 9-Fr introducer sheaths (Intro-Flex, Edwards Lifesciences, Dilbeek, Belgium) were placed for the introduction of 2 decapolar catheters positioned at: (1) the cranial side of the intervenous tubercle, with the tip curved against and directed toward the tubercle's base, and (2) the terminal crest, with the tip curved around it.

After SR recordings, APCs were induced at multiple locations by sequentially pacing (Micropace EPS320, Micropace EP Inc., Santa Ana, United States) via each decapolar catheter (electrodes 1-2) with a current of 15 mA, pulse width of 2 ms, and pacing rates of 45 and 120 beats per minute (bpm). Each pacing sequence lasted 10-20 beats. Care was taken to ensure that ectopic atrial depolarizations (P′ waves) were not obscured by QRS complexes or T waves. When necessary, the pacing rate was adjusted by $\pm$ 5 bpm to minimize superimposition.

Subsequently, a decapolar catheter was introduced through the 8.5-Fr bidirectional deflectable guiding sheath in the left jugular vein that had been used for the loop catheter, to pace at the right atrial free wall, right atrial appendage, fossa ovalis, intervenous tubercle, terminal crest, and caudal and cranial vena cava. Within the right atrium, the free wall was distinguished from the appendage using a combination of transthoracic echocardiography and 3D EAM. The interatrial septum was identified on a standard 4-chamber echocardiographic view, whereas the fossa ovalis was localized more precisely on a caudal echocardiographic plane. The clear anatomical landmarks enabled reliable differentiation of these nearby sites.

Finally, one of the decapolar catheters was inserted into the right ventricle, and VPCs were induced at pacing rates of 45 and 70 or 120 bpm, by pacing at the high and mid right ventricular free wall, the high and mid septum, the moderator band, the right ventricular apex, and the right ventricular outflow tract.

Left heart

Right heart procedures were performed in standing, sedated horses. After an interval of at least 4 weeks, the left heart was catheterized with the horse under general anesthesia because

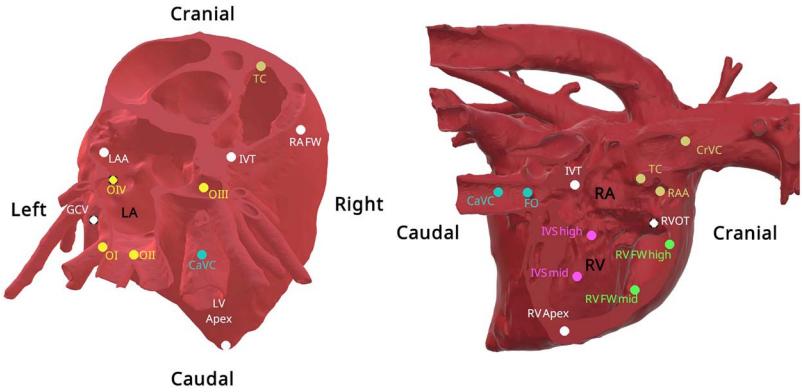

Figure 1 Overview of the paced locations in the LA, RA, and RV. The left image is a dorsal view optimized to visualize the 4 pulmonary vein ostia. The right image is a right lateral view of the heart, showing the paced locations in the RA and RV. Regions sharing the same color are grouped at the intermediate level of coarseness for further analysis. Abbreviations: CaVC = caudal vena cava; CrVC = cranial vena cava; FO = fossa ovalis; FW = free wall; GCV = great cardiac vein; IAS = interatrial septum (dorsal to the septal mitral valve leaflet); IVS = interventricular septum; IVT = intervenous tubercle; LA = left atrium; LAA = left atrial appendage; OI = ostium I; OII = ostium II; OIII = ostium III; OIV = ostium IV; RA = right atrium; RAA = right atrial appendage; RV = right ventricle; RVOT = right ventricular outflow tract; TC = terminal crest.

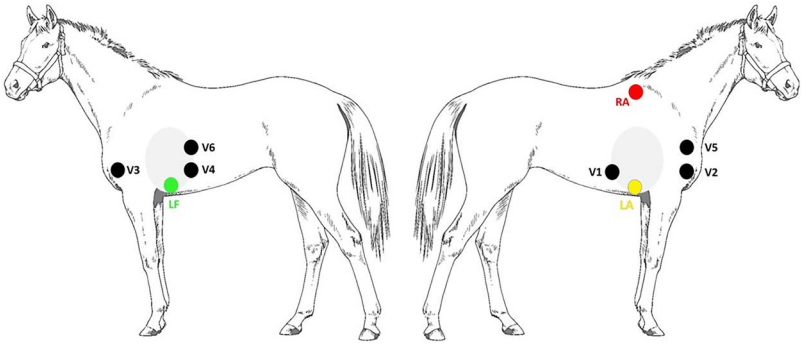

Figure 2 Positioning of the electrodes for the delta 12-lead configuration. The gray circle represents the cardiac contour. Abbreviations: LA = left arm electrode; LF = left foot electrode; RA = right arm electrode; V = precordial electrode.

the procedure required a transseptal puncture, a technique developed and validated under general anesthesia. Before induction of anesthesia, a fixed-curve sheath with a protruding J-tipped guidewire was inserted into the left jugular vein and positioned in the coronary sinus under transthoracic echocardiographic guidance. General anesthesia then was induced using a combination of ketamine (2.2 mg/kg) and midazolam (0.06 mg/kg) IV, and the horse was positioned in left lateral recumbency. Surface electrodes for the EnSite system and for a Δ 12-lead ECG were applied to shaved skin as described for the standing procedure.

The dilator and guidewire of the fixed-curve sheath were replaced with a decapolar deflectable catheter, which was advanced into the coronary sinus and the great cardiac vein. A 9-Fr introducer sheath, inserted via the right jugular vein, was used for insertion of an intracardiac echocardiography catheter (Acuson AcuNav 5.0-10.0 MHz, Biosense Webster, Diegem, Belgium). Under intracardiac echocardiographic guidance, a transseptal puncture was performed to allow placement of a deflectable guiding sheath into the LA via the right jugular vein.[13,18] Through this sheath, a 7-Fr loop electrophysiology catheter was introduced to obtain 3D EAM of the LA.

A decapolar catheter then was maneuvered into the LA to induce APCs by pacing (15 mA, 2 ms) at 45 and 120 bpm. Ectopy was induced sequentially at pulmonary vein ostia I-IV, the left atrial appendage, the fossa ovalis, within the great cardiac vein (at the level of the lateral left atrial free wall) and at the interatrial septum dorsal to the septal mitral valve leaflet.

Subsequently, a decapolar catheter was maneuvered into the left ventricle (LV) and VPCs were induced at pacing rates of 45 and 70 or 120 bpm by pacing at the high and mid left ventricular free wall, the high and mid septum, false tendon, left ventricular apex, and the left ventricular outflow tract. The left ventricular outflow tract (LVOT) position was defined as subaortic, directly beneath the aortic valve, and therefore was located more cranially than the high interventricular septum location, which was identified on a 4-chamber view and lay more caudally. In the left ventricle, a false tendon originating from the left bundle branch, visualized on a LVOT view, was selected for pacing in each horse.

At the end of the procedure, all catheters were withdrawn, and the horses were allowed to recover while being rope-assisted. The maximum allowed duration of anesthesia, including electrophysiological studies, was set at 5.5 h. After general anesthesia, enoxaparin (40 IU/kg SC q24; Clexane, Sanofi, Diegem, Belgium) was administered daily until transseptal puncture closure (median, 14 days; range, 1-35 days).[13]

Signal analysis

All signal processing, feature extraction, and classification analyses were performed using MATLAB (R2024b, The MathWorks,

Natick, MA, USA). Directional statistical analyses were conducted in R (Version 4.2.2, R Foundation for Statistical Computing, Vienna, Austria).

For each pacing location and speed, an operator (E.P.) manually selected and annotated 3 representative depolarizations for analysis. The onset of paced complexes was defined by the pacing stimulus artifact, whereas the manually selected P wave onset was used for SR beats. To facilitate inter-horse and inter-beat comparisons, the amplitude of all ECG signals for a given horse was normalized for visualization and automated classification. The normalization factor was derived from the maximum root-mean-square (RMS) amplitude of the 12 leads within a representative SR or paced complex from that same animal. Both P wave and QRS complex signals were scaled using this single, horse-specific factor. The 12-lead ECG subsequently was transformed into a 3D-VCG composed of orthogonal X, Y, and Z axes as previously described.[12]

Beat selection and feature extraction

All ECG and VCG signals were band-pass filtered between 1 and 100 Hz using a digital Butterworth filter. For each set of 3 manually selected P waves (for APCs) or QRS complexes (for VPCs), directional vectors (azimuth and elevation angles) were calculated for each depolarization. Azimuth angles represent the angle between the projection of the vector onto the X-Z plane and the positive X-axis (0° = left, +90° = caudal direction). Elevation angles represent the angle between the vector and the X-Z plane, with 0° indicating a vector within the plane and + 90° indicating a dorsal direction. All 3 beats were processed to eliminate selection bias.

For each depolarization, onset and offset were determined automatically. Onset was identified via pacing spike detection, and the offset was determined using a previously described algorithm.[19] In short, for the P wave, the end was identified as the point minimizing the sum of squared residual errors from each region's local mean, whereas for the QRS complex, it was identified as the intersection between the baseline and the tangent applied to the slurring part of the QRS complex. A 20 ms window, extending from 10 ms before to 10 ms after the pacing spike, was removed from the signal and replaced with linear interpolation across that window. Key VCG directional features were extracted, including:

- Initial vector: The direction of the largest local maximum within the first 40 ms of the P wave/QRS complex. If no distinct peak was found, the mean direction over this 40 ms interval was used.
- Mean vector: The direction corresponding to the maximum of the spatial RMS signal of the P wave/QRS complex.
- To ensure statistical independence (one observation per animal per location), the directional vectors of the 3 beats were vector-averaged to produce a single representative metric per horse for statistical testing.

Statistical analysis

Statistical analysis was performed using R statistical software. The QRS mean electrical axis (MEA) values (azimuth and elevation) measured from sinus beats during anesthesia and in the standing horse were converted into 3D Cartesian unit vectors. The resultant vector was calculated for each measurement, and the geodesic angular distance was computed for the pairwise combination within each horse. To evaluate the similarity of the QRS MEA between sedation and general anesthesia, a directional two one-sided test (TOST) was implemented using a bootstrapping procedure (n = 5000 resamples). The mean angular distance was compared against a zero-difference null hypothesis (significance testing) and a predefined equivalence bound of 5 degrees (equivalence testing). Confidence intervals (90% CI) were derived from the bootstrap distribution to determine both statistical significance and clinical equivalence.

Directional statistical analysis

Summary data, including directional vectors and timing metrics, were exported for statistical analysis in R. The initial and mean vectors of the P wave/QRS complex were converted from spherical to 3D Cartesian coordinates. To determine the appropriate statistical model for the directional data, the distribution of directional vectors for each pacing location was tested for conformity to a von Mises–Fisher (circularly symmetric) or Kent (elliptical) distribution using the Fishkent test. The concentration parameter (kappa), which quantifies the degree of vector clustering, then was estimated for each location. A directional analysis of variance (ANOVA), based on the likelihood ratio test, was employed to assess significant ($P < .05$) differences in the mean directional vectors between anatomical groups (eg, RA vs LA, RV vs LV) and pacing rates. To identify specific differences between individual pacing locations, post-hoc pairwise likelihood ratio tests were performed. To strictly control the family-wise error rate, all resulting P-values for these multiple comparisons were adjusted using the Bonferroni correction.

Pacing site classification using dynamic time warping (DTW)

A supervised machine learning classifier was developed in MATLAB to automatically identify the pacing origin based on signal morphology.

The classification relied on a template-matching approach using dynamic time warping (DTW),[20] an algorithm that measures the distances between 2 temporal sequences that may vary in time or speed.

a. Template generation: For each distinct pacing location, a template signal was created by averaging all 3 VCGs (or ECGs) from all horses for that specific site after aligning them with the maximal amplitude of the RMS signal.
b. Classification procedure: Each individual depolarization (all 3 per horse, test signal) was classified by computing its DTW distance to every site-specific template. The test signal was assigned the anatomical label of the template that yielded the minimum DTW distance.

In addition to distinguishing among all specific anatomical pacing sites, classification performance was evaluated across several levels of regional coarseness:

- Fine: Each distinct anatomical site was considered separately.
- Intermediate: Certain adjacent or functionally related pacing locations were grouped to represent broader regions: high and mid free wall sites, as well as septal sites, were grouped as free wall/septum. All ostial sites were analyzed

Table 1 Summary of the number of horses in which consistent capture was achieved at each pacing site in the RA, RV, LA, and LV.

RA (*n* = 8)		RV (*n* = 8)		LA (*n* = 7)		LV (*n* = 7)	
CaVC	7	Apex	7	Ostium I	5	Apex	6
FO	5	FW mid	6	Ostium II	4	FW mid	6
FW	7	FW high	5	Ostium III	6	FW high	6
IVT	6	IVS mid	6	Ostium IV	4	IVS mid	6
TC	6	IVS high	6	IAS	6	IVS high	6
RAA	5	MB	3	FO	3	FT	4
CrVC	6	RVOT	7	LAA	4	LVOT	6
				GCV	6		

These locations are grouped at the intermediate level of coarseness for further analysis: CaVC and FO; TC, RAA and CrVC; FW mid and high; IVS mid and high; all osteal sites. Abbreviations: CaVC = caudal vena cava; CrVC = cranial vena cava; FT = false tendon; FW = free wall; GCV = great cardiac vein; IAS = interatrial septum (dorsal to the septal mitral valve leaflet); IVS = interventricular septum; IVT = intervenous tubercle; LA = left atrium; LAA = left atrial appendage; LV = left ventricle; LVOT = left ventricular outflow tract; MB = moderator band; OF = fossa ovalis; OI = Ostium I; OII = Ostium II; OIII = Ostium III; OIV = Ostium IV; RA = right atrium; RAA = right atrial appendage; RV = right ventricle; RVOT = right ventricular outflow tract; TC = terminal crest.

as one group. The cranial vena cava, terminal crest, and right atrial appendage sites were combined, as were the RA fossa ovalis and caudal vena cava sites.
- Coarse: Only the main cardiac chambers were distinguished (ie, left vs right atrium/ventricle).

c. Performance evaluation: The classifier's performance was systematically evaluated under multiple conditions by varying:

- Signal type: Using either multichannel ECG or VCG data.
- Anatomical region: Classifying atrial and ventricular sites.
- Lead configuration: Using either the full signal set (12-lead ECG or 3D-VCG) or a smaller 2-channel set derived from the proposed Δ electrode configuration to simulate a simplified acquisition system (2D-VCG).

The performance was assessed using overall accuracy with 95% CI, and the weighted F1-score to account for class imbalances.

Results

Procedures went as planned, except for 1 horse in which the procedure under general anesthesia was prematurely interrupted because of hyperkalemia of unknown origin. The LA and LV were not paced in this horse. Pacing was sometimes ineffective because of insufficient wall contact resulting in non-capture. Catheter positioning was performed using transthoracic echocardiography and verified on 3D EAM. For each pacing site, we aimed to reproduce the same anatomical location as consistently as possible across horses. However, small variations in position might have occurred, because some target regions were relatively large or because precise localization was challenging (eg, the pacing location within a pulmonary vein might have been more lateral or medial, caudal, or cranial). An overview of the number of pacing sites with successful and good-quality capture is given in Table 1.

The analysis compared the spatial orientation of the MEA between standing and anesthetized positions. A significant difference was observed in the MEA orientation between the 2 positions, with a mean angular change of 2.82 degrees (90% CI, 1.71-2.89 degrees). Although the CI excluded zero, confirming a detectable shift ($P < .05$), the upper bound of the interval (2.89 degrees) remained well below the predefined equivalence margin of 5 degrees. Therefore, although a systematic difference was detected, the magnitude of the shift was statistically equivalent and considered not to be clinically relevant.

Because the directions of vectors for APCs and VPCs did not differ significantly between pacing rates of 45, 70, or 120 bpm ($P > .05$ for all locations), all subsequent analyses were performed using data obtained at a pacing rate of 45 bpm. Sinus rhythm beats were excluded from the dataset because their presence was found to degrade classification performance, probably because of substantial physiological variability in inter-horse P wave morphology during SR.

The azimuth and elevation angles of the initial (within first 40 ms) and mean directional vectors for each pacing site are presented in Table 2. Figure 3 illustrates 12-lead ECGs and VCG overlap plots of a pacing site with consistent waveforms and vector orientations across horses (mid LV free wall pacing) and of a pacing site for which the results varied between horses (caudal vena cava pacing) with variable waveforms and vector directions.

Directional analysis indicated no significant difference in initial vector directions between pacing sites ($P = .99$), whereas mean QRS vector directions differed significantly ($P < .001$). In contrast, for the P wave, both the initial vector directions and the mean vector directions over the entire wave differed significantly between pacing sites ($P < .001$ and $P = .007$, respectively).

The 3D-VCG achieved 99% (96%-100%) accuracy in distinguishing left- from right-sided origins (coarse level) of paced VPCs, whereas the 2D-VCG (based on the Δ configuration) also performed well, with an accuracy of 96% (93%-98%; Table 3). A similar trend was observed for paced APCs, with accuracies of 87% (82%-91%; 3D-VCG) and 78% (72%-83%; 2D-VCG). For intra-chamber localization into broader regions (intermediate level), accuracies were 76% (70%-81%) with the 3D-VCG vs 69% (63%-75%) with the 2D-VCG for the ventricles, and 65% (58%-71%) versus 53% (46%-60%) for the atria, respectively. Accuracy for localizing the precise pacing site was lower, 67% (60%-73%; 3D-VCG) vs 55% (48%-61%; 2D-VCG) in the ventricles, and 63% (57%-69%) vs 49% (42%-55%) in the atria. Origin localizations of ventricular depolarizations had a higher accuracy compared

Table 2 Directions of the initial (first 40 ms) and mean (the remainder of the P wave/QRS complex) depolarization vectors for each pacing site.

Pacing site		Az i		El i		Kappa	Az mean		El mean		Kappa
		Mean	SD	Mean	SD	Initial	Mean	SD	Mean	SD	Mean
SR	P wave	38	62	−27	21	4	49	18	−36	8	25
	QRS complex	28	92	16	46	1	−83	60	74	7	40
RA	CaVC	−41	24	−10	19	8	−65	47	−21	28	4
	FO	−18	48	−26	15	4	−32	67	−28	23	2
	FW	4	62	−11	21	0	49	28	−34	9	11
	IVT	−20	79	−47	15	4	32	20	−54	14	22
	TC	75	64	−14	36	2	61	65	−22	32	2
	RAA	58	9	−29	6	68	52	10	−39	2	104
	CrVC	77	10	−44	5	82	60	8	−42	5	107
RV	Apex	38	24	−2	27	6	−50	37	52	32	5
	FW mid	15	89	−2	33	1	16	11	−17	8	39
	FW high	70	59	−7	6	2	0	7	−23	8	62
	IVS mid	67	87	−9	21	1	18	31	−20	13	7
	IVS high	−32	30	−9	22	5	15	11	−29	10	33
	MB	58	72	−21	14	2	27	14	−29	15	20
	RVOT	16	97	−10	25	1	64	10	−13	13	26
LA	Ostium I	−107	31	−32	11	0	−46	83	−11	14	2
	Ostium II	−88	28	−37	22	7	−108	69	−8	30	1
	Ostium III	−1	40	−35	14	6	−1	76	−31	29	2
	Ostium IV	−125	86	−61	16	9	−100	56	−56	23	8
	IAS	50	29	3	22	6	−127	80	−21	20	4
	FO	3	23	−29	19	0	−47	70	−34	37	2
	LAA	140	134	−22	26	1	−85	15	−19	15	17
	GCV	−130	18	23	12	15	−91	27	−9	16	7
LV	Apex	−13	130	−8	28	1	−119	26	60	6	41
	FW mid	−47	65	1	14	2	−137	6	23	11	42
	FW high	−5	31	−22	16	7	−135	8	6	12	31
	IVS mid	14	57	−28	19	3	−97	77	43	39	2
	IVS high	82	30	−21	22	6	−96	11	2	34	6
	FT	47	50	−46	15	0	−115	20	48	12	20
	LVOT	78	46	−15	32	3	−72	66	−29	25	2

Azimuth angles represent the estimated angle between the projected vector in the X-Z plane and the positive X-axis, while elevation angles represent the angle between the vector and the X-Y plane with positive values denoting dorsally directed vectors. Kappa is a concentration parameter: higher values indicate greater concentration, lower indicates more spread. Abbreviations: Az i = azimuth initial; CaVC = caudal vena cava; CrVC = cranial vena cava; CS = coronary sinus; El i = elevation initial; FT = false tendon; FW = free wall; GCV = great cardiac vein; IAS = interatrial septum (dorsal to the septal mitral valve leaflet); IVS = interventricular septum; IVT = intervenous tubercle; LAA = left atrial appendage; LVOT = left ventricular outflow tract; OF = oval fossa; OI = Ostium I; OII = Ostium II; OIII = Ostium III; OIV = Ostium IV; RAA = right atrial appendage; RVOT = right ventricular outflow tract; SR = sinus rhythm; TC = terminal crest.

with those of atrial depolarizations, in all categories (coarse, intermediate, and fine). Interpretation of the 12-lead ECG itself achieved an accuracy of 88% (84%-92%) for APCs and 96% (93-98%) for VPCs at the coarse level. For intermediate localization, accuracy was 73% (67%-79%) with the 12-lead ECG compared to 64% (58%-70%) with the 3-lead ECG for ventricular origin, and 62% (55%-68%) vs 48% (41%-54%) for atrial origin. Accuracy decreased further for fine localization. Across all levels of coarseness, 3D-VCG facilitated visualization and interpretation of the ectopic foci compared with 12-lead ECG. The Δ configuration and 2D-VCG generally showed lower accuracy and weighted F1-scores compared with 12-lead recordings and 3D-VCG.

Figures 4 and 5 illustrate the mean VCG loop for each pacing location, emphasizing differences in vector trajectories when pacing at the various sites in the atria (Figure 4) and ventricles (Figure 5). The mean electrical axis (MEA) of the heart represents the average direction of the entire depolarization in 3D. In SR, the MEA of the P wave showed a left caudoventral direction and the QRS complex a craniodorsal direction. In general, APCs induced from the LA had a predominant right cranioventral direction, while those from the RA had a main left caudoventral direction. For APCs originating from the cranial vena cava, the MEA of the P wave was directed left caudoventrally, whereas pacing at the caudal vena cava induced a left cranially directed MEA. Pacing at the right atrial free wall, the intervenous tubercle, the right atrial appendage and the terminal crest also showed a mainly left caudoventrally directed MEA. Pacing the fossa ovalis from the LA and RA induced a left cranioventrally directed MEA. For most of the other pacing locations in the LA (ostia I, II, and IV; the interatrial septum dorsal to the septal mitral valve leaflet; and the left atrial appendage), the MEA was directed right-cranioventrally. Exceptions were observed at ostium III where the MEA was directed left-ventrally, and at the great cardiac vein where the MEA had a right cranial direction. Induced VPCs in the LV mid free wall, the apex and the false

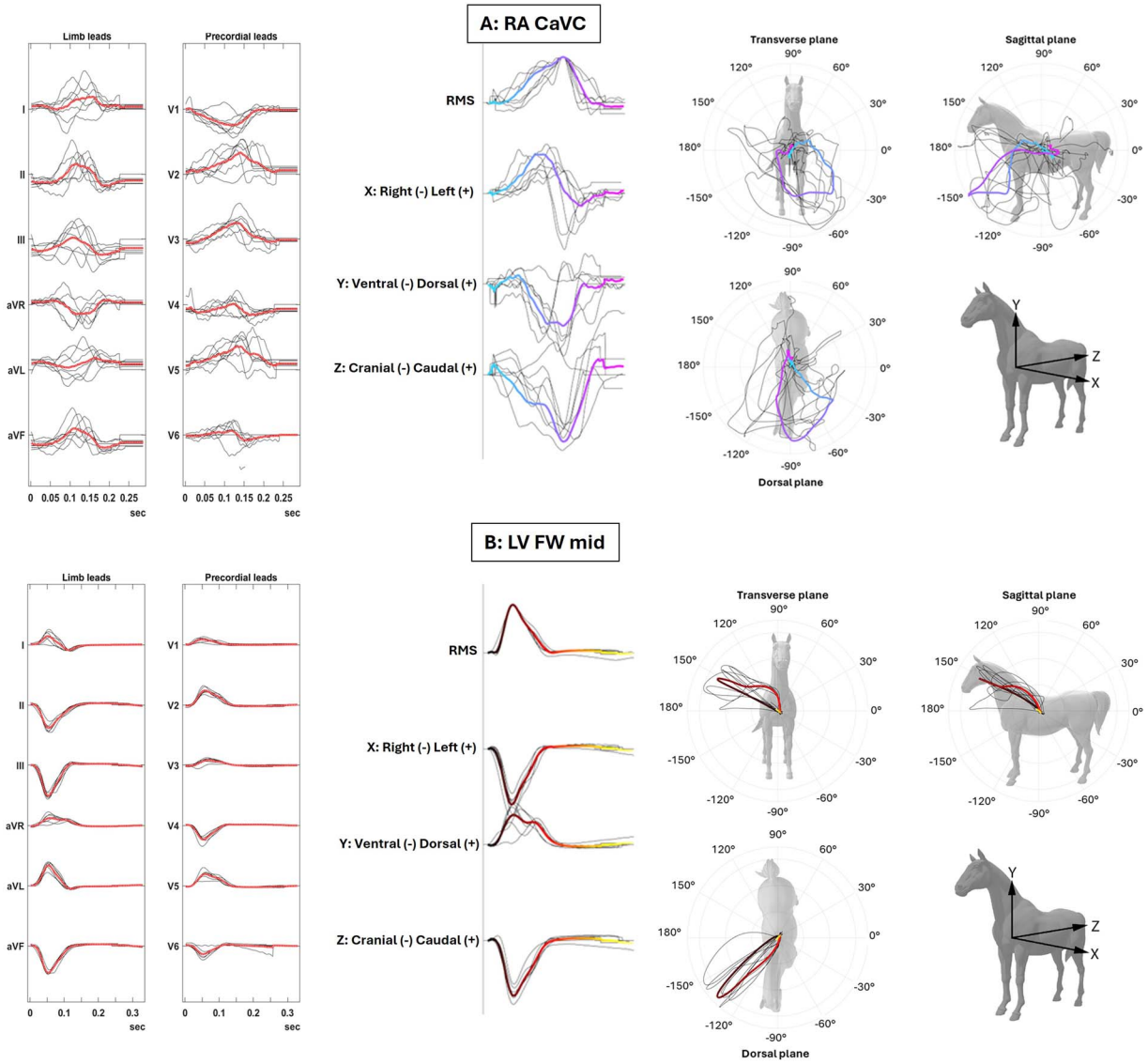

Figure 3 (A) P wave during atrial pacing at the caudal vena cava (RA CaVC) on the delta 12-lead ECG (left) and 3D-vectorcardiography (right). The VCG vector progresses from light blue to purple. (B) QRS complex during pacing at the mid LVFW on the delta 12-lead ECG (left) and 3D-vectorcardiography (right). The VCG vector progresses from yellow to dark red. Black lines are the individual results for each horse, colored lines are the mean results across all horses. At the level of the CaVC results varied between horses while the LVFW showed consistent results. Abbreviations: CaVC = caudal vena cava; LV FW = left ventricular free wall; VCG, vectorcardiography.

tendon had a right craniodorsal MEA. Induced VPCs in the high LV septum and free wall had a mainly cranial MEA, whereas the VPCs located at the mid LV septum had a dorsally aimed MEA. Pacing at the RV apex induced a left craniodorsally aimed MEA. Induced VPCs originating from the moderator band had a left caudoventrally aimed MEA. Induced VPCs from the RV outflow tract had a left caudoventrally to dorsally aimed MEA. Pacing at the RV free wall and septum induced a leftward MEA, initially directed caudoventrally and then shifting craniodorsally. An overview of the 12-lead ECG traces from all horses for all pacing sites is shown in Supplementary File S2.

Discussion

We describe the VCG characteristics of induced APCs and VPCs in horses by means of intracardiac pacing at 29 anatomical locations throughout the right and left atrium, and the right and left ventricle. The obtained graphs can be used for interpretation of VCGs in clinical cases.

The directions of vectors for APCs did not differ significantly between pacing rates (45 or 120 bpm). In horses, however, the morphology of the P wave during SR can be variable. The P waves may appear bifid, monophasic positive, or biphasic, and their configuration can change with heart rate or even between successive beats.[21] At lower heart rates, such variability may result from sinus arrhythmia or alterations in autonomic tone that influence conduction through the Bachmann bundle. The large atrial dimensions in horses and the potential presence of multiple interatrial conduction pathways may further contribute to asynchronous atrial activation. In addition, shifts in the exit site of impulse initiation within the sinus node region, which are modulated by autonomic tone, also can lead to beat-to-beat differences in P wave morphology.[22,23] At higher heart rates,

Table 3 Accuracy with 95% CI of origin classification at coarse (chamber-level), intermediate (regional grouping), and fine-grained levels using 2D- and 3D-VCG, or conventional ECG analysis based on either all 12 leads or the 3-lead delta configuration.

Type	Region	Classification	Leads used	Accuracy	Weighted F1 (%)
VCG	Atrial	Coarse	All	87% [82% 91%]	87
VCG	Atrial	Coarse	Delta	78% [72% 83%]	78
ECG	Atrial	Coarse	All	88% [84% 92%]	88
ECG	Atrial	Coarse	Delta	73% [66% 78%]	73
VCG	Atrial	Intermediate	All	65% [58% 71%]	61
VCG	Atrial	Intermediate	Delta	53% [46% 60%]	49
ECG	Atrial	Intermediate	All	62% [55% 68%]	59
ECG	Atrial	Intermediate	Delta	48% [41% 54%]	47
VCG	Atrial	Fine	All	63% [57% 69%]	62
VCG	Atrial	Fine	Delta	49% [42% 55%]	46
ECG	Atrial	Fine	All	60% [53% 66%]	56
ECG	Atrial	Fine	Delta	42% [36% 49%]	40
VCG	Ventricular	Coarse	All	99% [96% 100%]	99
VCG	Ventricular	Coarse	Delta	96% [92% 98%]	96
ECG	Ventricular	Coarse	All	96% [93% 98%]	96
ECG	Ventricular	Coarse	Delta	86% [81% 90%]	86
VCG	Ventricular	Intermediate	All	76% [70% 81%]	75
VCG	Ventricular	Intermediate	Delta	69% [63% 75%]	69
ECG	Ventricular	Intermediate	All	73% [67% 79%]	73
ECG	Ventricular	Intermediate	Delta	64% [58% 70%]	62
VCG	Ventricular	Fine	All	67% [60% 73%]	65
VCG	Ventricular	Fine	Delta	55% [48% 61%]	53
ECG	Ventricular	Fine	All	62% [56% 69%]	62
ECG	Ventricular	Fine	Delta	55% [48% 62%]	53

The weighted F1 score represents the weighted mean of sensitivity and specificity, adjusted for class distribution. Abbreviation: VCG = vectorcardiography.

changes in autonomic tone and more overlap of right and left atrial activation typically result in a single P wave.[24,25] During pacing maneuvers, such changes were not observed.

The potential influence of standing sedation versus general anesthesia on cardiac conduction was evaluated by comparison of P waves and QRS complexes of SR beats recorded during standing sedation and under general anesthesia. This evaluation identified only small differences in the MEA that were not considered clinically relevant.

Analysis of mean vector directions confirmed that pacing at different atrial and ventricular sites produced different and reproducible activation patterns (Table 2). The initial 40 ms vectors showed the strongest site-dependence, emphasizing their value for localizing the origin of activation. In contrast, the mean vectors of the entire P wave or QRS complex exhibited lower variability among horses. Even during SR, variability in mean vector directions was observed, which reflects the physiological heterogeneity of atrial and ventricular activation in horses.[24,26] During pacing, additional variation may arise from differences in electrical contact quality, slight changes in the exact position of the pacing catheter, and variation in the conduction pathway activated. For example, caudal vena cava pacing might have been performed at a more dorsolateral or more ventral site, and terminal crest pacing might have been with the pacing catheter more or less deep into the right atrial appendage, which could have affected mainly the initial activation pattern. Pacing the ventral wall of ostium III might favor conduction through the oval fossa. For LA ectopy, the RA activation pattern is dependent on the nature of left-to-right atrial conduction. In humans, the 3 major interatrial conduction routes described are via the Bachmann bundle, the oval fossa, and the coronary sinus musculature.[5] Similarly, in horses, breakthrough at the Bachmann bundle and a caudal breakthrough site have been documented on 3D EAM.[7] Morphological studies suggest right–left myocardial connections can exist between the coronary sinus and left atrium, and near the fossa ovalis, between right atrium and ostium III (Ibrahim L., unpublished data). Right-to-left atrial conduction therefore may vary among horses, which also can contribute to differences in VCG loop morphology.

For each pacing location, the initial vector from atrial pacing sites showed less variation than those from ventricular pacing sites, whereas the mean vectors were more consistent for ventricular pacing sites than for atrial ones. This pattern likely reflects differences in anatomy and conduction. In the atria, the initial depolarization is highly dependent on the precise pacing site, but once activation spreads, specific conduction pathways may introduce variability. In the ventricles, initial depolarization may vary more because of site-dependent breakthrough patterns, whereas overall conduction is less variable because it is dominated by the Purkinje system—which ensures rapid and transmural activation of the ventricular myocardium.[25,27–29]

Our findings are largely consistent with those of previous studies,[7,30] demonstrating that mean vector directions of the

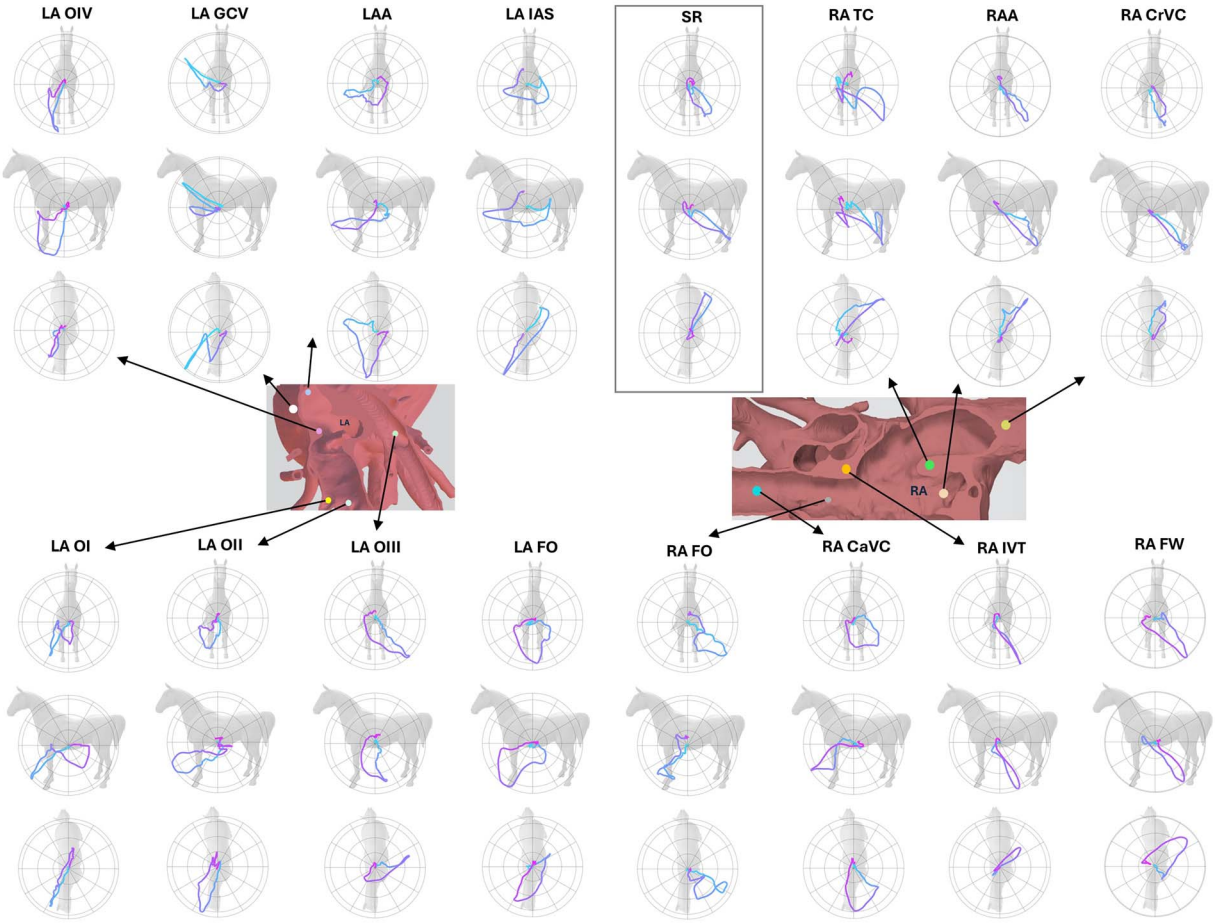

Figure 4 Mean atrial VCG loops with their respective locations of pacing in the LA and RA. The vector progresses from light blue to purple. Abbreviations: CaVC = caudal vena cava; CrVC = cranial vena cava; FO = fossa ovalis; FW = free wall; IAS = interatrial septum (dorsal to the septal mitral valve leaflet); IVS = interventricular septum; IVT = intervenous tubercle; LA = left atrium; LAA = left atrial appendage; OI = ostium I; OII = ostium II; OIII = ostium III; OIV = ostium IV; RA = atrium; RAA = right atrial appendage; RVOT = right ventricular outflow tract; TC = terminal crest; VCG = vectorcardiogram.

VCG correspond with the pacing site and form reproducible, location-specific patterns. Despite differences in electrode positioning among the studies, the main vector directions followed comparable trajectories, supporting the notion that VCG provides robust and reproducible activation patterns that are less dependent on electrode placement. Whereas the 3D-VCG system provided the highest spatial resolution and overall diagnostic accuracy, the simplified 2D-VCG approach also achieved excellent discrimination between left- and right-sided origins of APCs and VPCs. The balance between practicality and diagnostic accuracy emphasizes the potential of the Δ 2D-VCG as a clinically applicable, initial diagnostic tool. Moreover, direct interpretation of the polarity of the depolarization wave on each of the 3 leads of the ECG provides direct information about the mean direction of depolarization. Standardized use of the Δ configuration could enhance cross-center comparability and provide more insight into the contribution of arrhythmias to poor performance and sudden cardiac death in horses. In addition, the Δ 12-lead configuration, derived from a base-down Einthoven triangle with 4 precordial electrodes positioned at mid-ventricular level and 2 precordial electrodes near the right and left atrium, offers additional advantages. It allows enhancement of P wave amplitude, thereby improving recognition of supraventricular arrhythmias, and the close positioning of precordial leads to cardiac chambers provides high sensitivity for identifying the anatomical origin of both atrial and ventricular arrhythmias.

The noninvasive 12-lead technique can be performed in the standing, non-sedated horse, which is clinically relevant because it may facilitate better understanding of arrhythmias and potential arrhythmogenic areas in the heart, but also in selecting an optimal treatment strategy, such as ablation.[31] With prior knowledge of the likely region of interest within the atria or ventricles, catheters can be targeted immediately to the correct compartment during anesthesia, minimizing the need for extensive mapping and, thereby, limiting anesthesia time. This approach could decrease anesthesia-related risks while maintaining therapeutic efficacy.[16,32,33] Performing 12-lead ECG and VCG in a larger cohort of horses with naturally occurring arrhythmias would enable better identification of arrhythmogenic regions and chamber-specific conduction abnormalities, but also facilitate development of horse-specific ablation strategies. Beyond the role in guiding interventional procedures, standardized use of 12-lead ECG and VCG in equine cardiology could provide valuable diagnostic and prognostic information across a wide range of conditions, including the differentiation of benign from malignant arrhythmias, risk stratification for

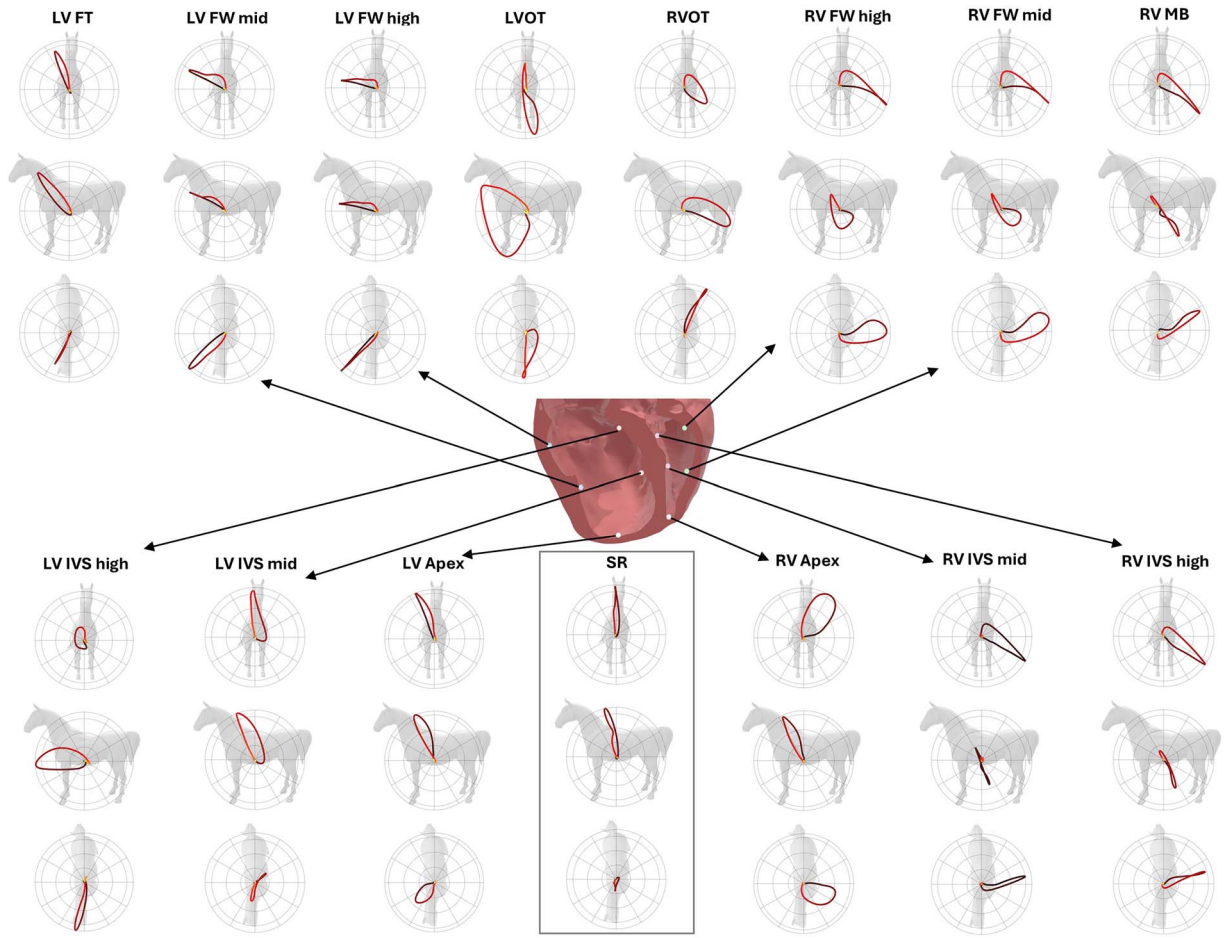

Figure 5 Mean ventricular VCG loops with their respective locations of pacing in the LV and RV. The vector progresses from yellow/light red to dark red. Abbreviations: FT = false tendon; FW = free wall; IVS = interventricular septum; LV = left ventricle; LVOT = left ventricular outflow tract; MB = moderator band; RV = right ventricle; RVOT = right ventricular outflow tract; VCG = vectorcardiogram.

sudden cardiac death, and assessment of electrical remodeling in structural heart disease. Furthermore, VCG has the unique advantage of generating 3D representations of electrical activity by combining information from different electrodes, thereby offering robust and reproducible activation patterns even under variable clinical conditions. Both techniques provide considerably more information than what is currently available from most ECG recordings. Using a standardized electrode placement and analysis is essential to fully exploit the diagnostic and prognostic potential of 12-lead ECG and VCG in horses.

Our study had some limitations. Only a small number of horses was included, and all premature complexes were pacing-induced. The applicability of these findings to naturally occurring arrhythmias remains to be demonstrated. Although 8 horses were included, several pacing locations were represented by data from only 3 to 4 horses (Table 1). No formal power analysis was performed for discrimination across the 29 pacing sites, and the study was, therefore, exploratory in nature. As a result, conclusions regarding fine-grained localization should be interpreted with caution and warrant confirmation in larger cohorts with more uniform site representation. Substantial class imbalance existed across pacing sites. Templates for sparsely represented locations are inherently less representative, and DTW-based distance calculations may be biased toward well-represented classes. Although weighted F1-scores partially address this issue, class imbalance particularly affects fine-grained classification, which is therefore less clinically robust than chamber-level or regional discrimination. Site-specific sensitivity and specificity could not be estimated reliably for sparsely represented classes, limiting clinical interpretability at the finest level of localization. In addition, despite the use of echocardiography and 3D EAM to guide and verify catheter placement, it was not always possible to reproduce pacing sites at exactly the same anatomical location across different horses. This difficulty was mainly a consequence of the relatively large area of some target regions and the practical difficulty of achieving identical positioning within specific anatomical structures. This situation may have contributed to some variability in the recorded vectors. Furthermore, only healthy horses were included. Horses with structural cardiac abnormalities, such as areas of fibrosis, may display altered conduction patterns, which could influence VCG loop morphology and classification accuracy. Future studies, therefore, should validate our results in clinical cases, including horses with structural heart disease and spontaneous premature complexes.

In conclusion, we demonstrated that 3D-VCG based on the Δ 12-lead configuration enables noninvasive localization of focally induced premature complexes in horses, with nearly 99% accuracy for chamber-level discrimination, whereas the 3-lead Δ configuration is a simplified but promising and more practical technique. Fine-grained localization remains challenging, even

with the Δ 12-lead ECG, particularly for atrial origins. In such situations, a multiple-catheter intracardiac recording might provide additional details.[14]

Author contributions

Ellen Paulussen (Conceptualization, Data curation, Formal analysis, Investigation, Methodology, Project administration, Validation, Visualization, Writing—original draft), Gunther van Loon (Conceptualization, Data curation, Funding acquisition, Investigation, Methodology, Supervision, Writing—review & editing), Eva Buschmann (Data curation, Funding acquisition, Investigation, Writing—review & editing), Ingrid An Lucie Vernemmen (Funding acquisition, Investigation, Writing—review & editing), Tammo Delhaas (Conceptualization, Methodology, Writing—review & editing), Annelies Decloedt (Investigation, Supervision, Writing—review & editing), and Glenn Van Steenkiste (Conceptualization, Data curation, Formal analysis, Investigation, Methodology, Software, Supervision, Validation, Visualization, Writing—review & editing)

Supplementary material

Supplementary material is available at *Journal of Veterinary Internal Medicine* online.

Conflicts of interest

The authors declare no conflicts of interest.

Funding

Eva Buschmann and Ingrid Vernemmen were PhD fellows funded by the Research Foundation Flanders (FWO-Vlaanderen) (Grant numbers 1SE9122N and 1S71521N, respectively). Funding was received for ultrasound equipment by Special Research Fund Ghent University (Grant number 01B05818).

Off-label antimicrobial declaration

The authors declare no off-label use of antimicrobials.

Institutional animal care and use committee or other approval declaration

Procedures on animals were approved by the Ethical Committee, Faculty of Veterinary Medicine, Ghent University (EC2020/065). All experiments were performed in accordance with the relevant guidelines and regulations.

Human ethics approval declaration

The authors declare human ethics approval was not needed.

References

1. Zeppenfeld K, Tfelt-Hansen J, de Riva M, et al. 2022 ESC guidelines for the management of patients with ventricular arrhythmias and the prevention of sudden cardiac death: developed by the task force for the management of patients with ventricular arrhythmias and the prevention of sudden cardiac death of the European Society of Cardiology (ESC) endorsed by the Association for European Paediatric and Congenital Cardiology (AEPC). *Eur Heart J*. 2022;43:3997-4126. https://doi.org/10.1093/eurheartj/ehac262
2. Nath L, Stent A, Elliott A, la Gerche A, Franklin S. Risk factors for exercise-associated sudden cardiac death in thoroughbred racehorses. *Animals*. 2022;12:1297. https://doi.org/10.3390/ani12101297
3. Navas de Solis C. Exercising arrhythmias and sudden cardiac death in horses: review of the literature and comparative aspects. *Equine Vet J*. 2016;48:406-413. https://doi.org/10.1111/evj.12580
4. Vernemmen I, Buschmann E, Demeyere M, et al. Feasibility of transthoracic echocardiographic guidance for multicatheter electrophysiological mapping studies in horses. *J Vet Intern Med*. 2024;38:2686-2697. https://doi.org/10.1111/jvim.17156
5. van Loon G, Decloedt A. Arrhythmias and abnormalities of the cardiac conduction system in athletic horses. *Equine Sports Medicine and Surgery.* 3rd ed. Saunders Ltd.; 2024:831-865. https://doi.org/10.1016/B978-0-7020-8370-9.00038-2.
6. Hesselkilde EM, Isaksen JL, Petersen BV, et al. A novel approach for obtaining 12-lead electrocardiograms in horses. *J Vet Intern Med*. 2021;35:521-531. https://doi.org/10.1111/jvim.15980
7. Van Steenkiste G, Delhaas T, Hermans B, et al. An exploratory study on vectorcardiographic identification of the site of origin of focally induced premature Depolarizations in horses, part I: the atria. *Animals*. 2022;12:549. https://doi.org/10.3390/ani12050549
8. Orsini JA, Divers TJ. *Equine Emergencies E-Book: Treatment and Procedures*. Elsevier; 2013.
9. Van Zijl W. The electrocardiogram of the normal horse. *Acta Physiol Pharmacol Neerl*. 1954;3:435-436. Pubmed.ncbi.nlm.nih.gov/13228087/
10. Fregin G. The equine electrocardiogram with standardized body and limb positions. *Cornell Vet*. 1982;72:304-324. Pubmed.ncbi.nlm.nih.gov/7105763/
11. Buss DD, Rawlings CA, Bisgard GE. The normal electrocardiogram of the domestic pony. *J Electrocardiol*. 1975;8:167-172. https://doi.org/10.1016/S0022-0736(75)80025-2
12. Paulussen E, Delhaas T, Decloedt A, van Loon G, van Steenkiste G. Vectorcardiography at rest and during exercise in horses using the delta (Δ) 12-lead configuration. *J Vet Intern Med*. 2025;40:1-12. https://doi.org/10.1093/jvimsj/aalaf008
13. Vernemmen I, Buschmann E, Van Steenkiste G, et al. Intracardiac ultrasound-guided transseptal puncture in horses: outcome, follow-up, and perioperative anticoagulant treatment. *J Vet Intern Med*. 2024;38:2707-2717. https://doi.org/10.1111/jvim.17158
14. Buschmann E, Van Steenkiste G, Vernemmen I, et al. Multiple catheter recording in horses to investigate atrial depolarization pattern during sinus rhythm and induced premature atrial complexes. *J Vet Intern Med*. 2025;39:e70218. https://doi.org/10.1111/jvim.70218
15. Vernemmen I, Vera L, Van Steenkiste G, et al. Reference values for 2-dimensional and M-mode echocardiography in Friesian and warmblood horses. *J Vet Intern Med*. 2020;34:2701-2709. https://doi.org/10.1111/jvim.15938

16. Buschmann E, Van Steenkiste G, Vernemmen I, et al. Caudal vena cava isolation using ablation index-guided radiofrequency catheter ablation (CARTO™ 3) to treat sustained atrial tachycardia in horses. *J Vet Intern Med*. 2025;39:e17251. https://doi.org/10.1111/jvim.17251
17. Ibrahim L, Buschmann E, van Loon G, Cornillie P. Morphological evidence of a potential arrhythmogenic substrate in the caudal and cranial vena cava in horses. *Equine Vet J*. 2025;57:256-264. https://doi.org/10.1111/evj.14075
18. Vernemmen I, Van Steenkiste G, Buschmann E, et al. Development of an atrial transseptal puncture procedure in horses to access the left heart: an ultrasound-guided jugular vein and transhepatic approach. *Equine Vet J*. 2025;57:243-255. https://doi.org/10.1111/evj.14084
19. Paulussen E, Van Steenkiste G, Hermans BJ, et al. Einthoven's triangle adapted for horses: proposal for the delta configuration. *J Vet Intern Med*. 2024;38:2698-2706. https://doi.org/10.1111/jvim.17179
20. Paliwal KK, Agarwal A, Sinha SS. A modification over Sakoe and Chiba's dynamic time warping algorithm for isolated word recognition. *Signal Process*. 1982;4:329-333. https://doi.org/10.1016/0165-1684(82)90009-3
21. Verheyen T, Decloedt A, De Clercq D, et al. Electrocardiography in horses—part 1: how to make a good recording. *Vlaams Diergeneeskd Tijdschr*. 2010;79:331-336. https://doi.org/10.21825/vdt.87463
22. Muylle E. *Experimenteel Onderzoek naar het Verloop van de Depolarisatiegolf in het Hart van het Paard. De Genesis van het Electrocardiografisch P-en QRS-complex*. Mededelingen van de Faculteit Diergeneeskunde Rijksuniversiteit Gent (Belgium); 1975:19:1-177.
23. Schwarzwald CC, Hamlin RL, Bonagura JD, Nishijima Y, Meadows C, Carnes CA. Atrial, SA nodal, and AV nodal electrophysiology in standing horses: normal findings and electrophysiologic effects of quinidine and diltiazem. *J Vet Intern Med*. 2007;21:166-175. https://doi.org/10.1111/j.1939-1676.2007.tb02943.x
24. Marr C, Bowen M. *Cardiology of the Horse*. Elsevier Health Sciences; 2011.
25. Van Steenkiste G, Vera L, Decloedt A, et al. Endocardial electro-anatomic mapping in healthy horses: normal sinus impulse propagation in the left and right atrium and the ventricles. *Vet J*. 2020;258:105452. https://doi.org/10.1016/j.tvjl.2020.105452
26. Reef V, Bonagura J, Buhl R, et al. Recommendations for management of equine athletes with cardiovascular abnormalities. *J Vet Intern Med*. 2014;28:749-761. https://doi.org/10.1111/jvim.12340
27. Durrer D, Van Dam RT, Freud G, et al. Total excitation of the isolated human heart. *Circulation*. 1970;41:899-912. https://doi.org/10.1161/01.CIR.41.6.899
28. Ohkawa S. Distribution of Purkinje cells in hearts of human and various animals. *J Arrhythmia*. 2008;24:177-179. https://doi.org/10.1016/S1880-4276(08)80026-9
29. Bishop SP, Cole CR. Morphology of the specialized conducting tissue in the atria of the equine heart. *Anat Rec*. 1967;158:401-415. https://doi.org/10.1002/ar.1091580405
30. Van Steenkiste G, Delhaas T, Hermans B, et al. An exploratory study on vectorcardiographic identification of the site of origin of focally induced premature depolarizations in horses, part II: the ventricles. *Animals*. 2022;12:1-11. https://doi.org/10.3390/ani12050550
31. Buschmann E, Van Steenkiste G, Bulckens H, et al. Three-dimensional electro-anatomical mapping of premature atrial complexes originating from the right atrial free wall and treatment by radiofrequency ablation in three horses. *Equine Vet J*. 2025;56:1-9. https://doi.org/10.1111/evj.70095
32. Buschmann E, Van Steenkiste G, Vernemmen I, et al. Lesion size index-guided radiofrequency catheter ablation using an impedance-based three-dimensional mapping system to treat sustained atrial tachycardia in a horse. *Equine Vet J*. 2025;57:1009-1016. https://doi.org/10.1111/evj.14424
33. Van Steenkiste G, Boussy T, Duytschaever M, et al. Detection of the origin of atrial tachycardia by 3D electro-anatomical mapping and treatment by radiofrequency catheter ablation in horses. *J Vet Intern Med*. 2022;36:1481-1490. https://doi.org/10.1111/jvim.16473

Journal of Veterinary Internal Medicine, 2026, 40, 1–12
https://doi.org/10.1093/jvimsj/aalag080
Original Research